

A Stimuli Responsive System of Self-Assembled Anion-Binding $\text{Fe}_4\text{L}_6^{8+}$ Cages

Jack K. Clegg,^{†*} Jonathan Cremers,[†] Andrew J. Hogben,[†] Boris Breiner,[†] Maarten M. J. Smulders,[†] John D. Thoburn,^{†§} and Jonathan R. Nitschke^{†*}

[†] Department of Chemistry, The University of Cambridge, Lensfield Rd, Cambridge, CB2 1EW, United Kingdom.

[‡] School of Chemistry and Molecular Biosciences, The University of Queensland, Brisbane St Lucia, QLD, Australia, 4072.

[§] Department of Chemistry, Randolph-Macon College, Ashland, VA 23005, USA

*Correspondence to: either J. K. Clegg, j.clegg@uq.edu.au or J. R. Nitschke, jrn34@cam.ac.uk

Supporting Information

1. Experimental	2
1.1 General	2
1.1.1 4,4'-diaminobiphenyl	2
1.1.2 Hexakis(acetonitrile)iron(II) hexafluorophosphate	3
1.2 General synthesis of 1	3
1.2.1 [1]·8NTf ₂	3
1.2.2 [1]·8OTf·7H ₂ O	4
1.2.3 [PF ₆ ⊂1]·7PF ₆ ·3H ₂ O	4
1.2.4 [ClO ₄ ⊂1]·7ClO ₄ ·12H ₂ O	5
1.2.5 [BF ₄ ⊂1]·7BF ₄ ·3MeCN	5
1.3 Additional characterization details	6
1.3.1 Xray structure of Hexakis(acetonitrile)iron(II) hexafluorophosphate	6
1.3.2 Additional characterization for [1]·8NTf ₂	7
1.3.3 Additional characterization for [BF ₄ ⊂1]·7BF ₄	9
1.3.4 Additional characterization for [PF ₆ ⊂1]·7PF ₆	10
1.4 Crystallography	11
1.4.1 [Fe(MeCN) ₆]·2PF ₆	11
1.4.2 [I⊂1-T]·3I·3.5OTf·0.5NTf ₂ ·2MeCN·Et ₂ O	11
1.4.3 [1-S ₄]·8NTf ₂ ·5MeCN·2H ₂ O·Et ₂ O	12
1.4.4 [PF ₆ ⊂1-T]·7PF ₆ ·9MeCN·3Et ₂ O	13
1.4.5 [ClO ₄ ⊂1-T]·4ClO ₄ ·3OTf·4MeCN·2Et ₂ O	13
1.4.6 [BF ₄ ⊂1-T]·7BF ₄ ·5.25MeCN·0.25Et ₂ O	14
1.5 Titrations	15
1.5.1 Method for direct titration	15
1.5.2 Method for the competitive displacement of PF ₆ by bromide	15
1.5.3 Method for relative binding investigations	15
1.5.4 Derivation of binding model guest encapsulation in the system of 1	16
1.5.5 Curves obtained for direct titration of I ⁻ , BF ₄ ⁻ and ClO ₄ ⁻ , each showing strong binding	19
1.5.6 Data fitting for direct titration of PF ₆ ⁻ into I ⁸⁺	21
1.5.7 Data fitting for competitive titration of Br ⁻ against PF ₆ ⁻	21

1.6	Molecular Modelling and Anion Volume Calculations.....	22
1.7	Volume calculations.....	22
1.8	Kinetics.....	23
1.8.1	PF ₆ ⁻ diastereomer exchange.....	23
1.8.2	NTf ₂ ⁻ diastereomer exchange.....	27
1.8.3	BF ₄ ⁻ guest exchange monitored by 2D ¹⁹ F EXSY.....	28
1.8.4	Kinetics of PF ₆ ⁻ addition to [1- S ₄] ⁻ ·8NTf ₂	31
1.9	References.....	32

1. Experimental

1.1 General

All reagents and solvents were purchased from commercial sources and used as supplied unless otherwise mentioned. Iron(II) triflimide was prepared following a literature procedure.^{S1} NMR spectra were recorded on a Bruker Avance DPX400 or DPX500 spectrometer. Proton chemical shift (δ H) values are reported relative to the solvent residual peak (1.96 ppm for acetonitrile); δ F values are reported relative to 1,4-difluorobenzene at -121.4 ppm. Peaks are labelled according to the lettering shown in Figure 1 and *T*:*S*₄:*C*₃ ratios as reported in Table 1. Electrospray ionization mass spectra (ESI-MS) were obtained on a Micromass Quattro LC, infused from a Harvard Syringe Pump at a rate of 10 μ L per minute. The melting point is reported uncorrected. All samples for microanalysis were crushed and dried under vacuum for 24 hours over P₂O₅ prior to analysis.

1.1.1 4,4'-diaminobiphenyl.

4,4'-diaminobiphenyl was prepared by adaptation of a literature procedure.^{S2} Hydrazobenzene (5.0 g, 27.1 mmol, 1 eq.) was dissolved in a mixture of ethanol (150 mL) and water (50 mL) and cooled to 0 °C. Concentrated hydrochloric acid (20 mL, 57.4 mmol, 2 eq.) was diluted in water (80 mL) and ethanol (220 mL). The diluted hydrochloric acid solution was added to the hydrazobenzene solution at 0 °C. The mixture was allowed to warm to room temperature and stirred for 24 hours. Two thirds of the solvent was removed and cooled on ice to produce white crystals which were collected by filtration. The crystals were dissolved in 200 mL of water and the solution was neutralized with saturated aqueous sodium bicarbonate before extraction with dichloromethane (300 mL). The organic layer was separated and the aqueous layer was further extracted with dichloromethane (3x50 mL). The organic extracts were combined, dried over MgSO₄, and the solvent was removed to give a brown solid. Purification by recrystallization from water gave benzidine (2.95 g, 16.0 mmol, 59%) as white crystals. ¹H NMR and melting point matched the literature reports. ¹H NMR (400 MHz, 298 K,

CD₃CN): δ 7.28 (2H, d, J = 8.63 Hz), 6.66 (2H, d, J = 8.63 Hz), 4.10 (2H, s). m.p. 122-125 °C.

1.1.2 Hexakis(acetonitrile)iron(II) hexafluorophosphate.

While this salt is not commercially available due to decomposition, we found that it could be reliably stored in a plastic vial in a desiccator for several months. Hexakis(acetonitrile)iron(II) hexafluorophosphate was prepared by adaptation of a literature procedure.^{S3} Iron (105 mg, 1.88 mmol) and nitrosyl hexafluorophosphate (620 mg, 3.54 mmol) were added to distilled MeCN (50 mL) in a flame dried schlenk tube. The mixture was freeze dried and left to react overnight at room temperature. The reaction mixture was filtered to give a yellow solution which was concentrated to give a white solid. The white solid was recrystallized by dissolving in a minimum amount of distilled MeCN filtered to remove remaining solid and layered with distilled Et₂O to yield colorless needles (806 mg, 77%). ¹⁹F NMR (376 MHz, 298 K, CD₃CN): δ = -71.42 ppm (d, J = 706.7 Hz); ³¹P NMR (162 MHz, 298 K, CD₃CN): δ = -143.6 ppm (heptet, J = 706.7 Hz); Elemental Analysis (%) calcd for FeP₂F₁₂·6CH₃CN: C 21.80; H, 2.74; N, 12.71; found: C 21.90; H 2.75; N 12.67.

1.2 General synthesis of 1.

4,4'-diaminobiphenyl (100 mg, 0.54 mmol), 2-formylpyridine (103 μ L, 1.09 mmol) and the appropriate Fe(II)-salt (0.36 mmol) were dissolved in acetonitrile (50 mL). The reaction mixture was heated overnight at 50 °C under nitrogen. Diethyl ether (250 mL) was added. The purple microcrystalline powder was collected and subjected to size exclusion chromatography (Sephadex LH 20, H₂O:MeCN (3:7, v:v)). The purple band was collected and dried over MgSO₄. After filtration, a deep purple microcrystalline powder was precipitated with excess diethyl ether and collected.

1.2.1 [1]·8NTf₂.

Yield 376 mg, 90 %. ¹H NMR (400 MHz; 298 K; CD₃CN): δ 11.25 (1H, s, H^c (T)), 10.94 (1H, s, H^c (C₃)), 10.06 (1H, s, H^c (S₄)), 10.05 (1H, s, H^c (S₄)), 9.70 (1H, s, H^c (S₄)), 9.42 (1H, s, H^c (C₃)), 9.24 (1H, d, J = 7.40 Hz, H^d (T)), 9.17 (1H, d, J = 7.71 Hz, H^d (C₃)), 9.10 (1H, s, H^c (C₃)), 9.06 (1H, s, H^c (C₃)), 8.95 (1H, d, J = 7.25 Hz, H^d (S₄)), 8.81 (1H, d, J = 7.73 Hz, H^d (S₄)), 8.78 (1H, d, J = 7.94 Hz, H^d (S₄)), 8.71 (1H, d, J = 7.83 Hz, H^d (C₃)), 8.62 (1H, d, J = 7.18 Hz, H^d (C₃)), 8.59-8.24 (7H, H^e (3S₄, 4C₃)), 8.31 (1H, t, J = 7.79, H^e (T)), 8.20-8.03 (8H, H^f (T, 3S₄, 4C₃)), 7.97-7.70 (8H, H^g (T, 3S₄, 4C₃)), 7.70-7.38 (14H, H^a (3S₄, 4C₃)), 7.51 (2H, d, J = 7.57 Hz, H^a (T)), 5.90-5.40 (14H, H^b (3S₄, 4C₃)), 5.63 (2H, d, J = 7.82 Hz, H^b (T)). ¹⁹F NMR (376 MHz; 298 K; CD₃CN): δ -80.4

(s, NTf₂⁻). *m/z* (ESI-MS) = 879.64 [**1** + (NTf₂⁻)₄]⁴⁺, 1266.23 [**1** + (NTf₂⁻)₅]³⁺. Elemental Analysis (%) calcd for C₁₆₀H₁₀₈F₄₈Fe₄N₃₂O₃₂S₁₆: C, 41.42%; H, 2.35%; N, 9.66%. Found: C, 41.40%; H, 2.45%; N, 9.73%.

1.2.2 [1]·8OTf·7H₂O.

Yield 334 mg, 85 %. ¹H NMR (500 MHz; 298 K; CD₃CN): δ 11.51 (1H, s, H^c (S₄)), 11.31 (1H, s, H^c (T)), 11.13 (1H, s, H^c (C₃)), 10.09 (1H, s, H^c (C₃)), 10.00 (1H, s, H^c (S₄)), 9.67 (1H, s, H^c (S₄)), 9.46 (1H, s, H^c (C₃)), 9.32 (1H, d, *J* = 7.28 Hz, H^d (S₄)), 9.27 (1H, d, *J* = 7.43 Hz, H^d (T)), 9.08 (1H, s, H^c (C₃)), 8.97 (1H, d, *J* = 7.43 Hz, H^d (S₄)), 8.80 (1H, d, *J* = 7.28 Hz, H^d (S₄)), 9.36-8.67 (4H, H^d (C₃)), 8.68-8.22 (7H H^e (3S₄, 4C₃)), 8.31 (2H, t, *J* = 7.67 Hz, H^e (T)), 8.17-8.00 (8H, H^f (T, 3S₄, 4C₃)), 8.00-7.77 (8H, H^g (T, 3S₄, 4C₃)), 7.77-7.42 (C₃ peaks for H^a), 7.74 (2H, d, *J* = 7.38 Hz, H^a (S₄)), 7.64 (2H, d, *J* = 7.61 Hz, H^a (S₄)), 7.53 (2H, d, *J* = 6.97 Hz, H^a (T)), 7.49 (2H, d, *J* = 7.93 Hz, H^a (S₄)), 5.92 (2H, H^b (S₄)), 5.84 (2H, d, *J* = 7.60 Hz, H^b (C₃)), 5.73 (2H, d, *J* = 7.42 Hz, H^b (C₃)), 5.70 (2H, d, *J* = 7.98 Hz, H^b (C₃)), 5.66 (2H, d, *J* = 6.99 Hz, H^b (T)), 5.60 (2H, d, *J* = 7.42 Hz, H^b (C₃)), (4H, d, *J* = 8.20 Hz, H^b (2S₄)). ¹⁹F NMR (376 MHz; 298 K; CD₃CN): δ -79.5 (s, OTf⁻). *m/z* (ESI-MS) = 749.37 [**1** + (OTf⁻)₄]⁴⁺, 1048.48 [**1** + (OTf⁻)₅]³⁺. Elemental Analysis (%) calcd for C₁₅₂H₁₀₈F₂₄Fe₄N₂₄O₂₄S₈·7H₂O: C, 49.12%; H, 3.31%; N, 9.04%. Found: C, 48.69%; H, 3.15%; N, 9.12%.

1.2.3 [PF₆⁻1]·7PF₆·3H₂O.

Yield 325 mg, 86 %. ¹H NMR (400 MHz; 298 K; CD₃CN): δ 9.49 (1H, s, H^c (T)), 9.42 (1H, s, H^c (C₃)), 9.18 (1H, s, H^c (C₃)), 9.00 (1H, s, H^c (C₃)), 8.94 (2H, s, H^c (C₃, S₄)), 8.87 (2H, s, H^c (2S₄)), 8.74-8.50 (7H, H^d (3S₄, 4C₃)), 8.64 (1H, d, *J* = 7.61 Hz, H^d (T)), 8.47-8.26 (14H, H^e (3S₄, 4C₃) and H^f (3S₄, 4C₃)), 8.34 (2H, m, H^e (T) and H^f (2T)), 7.96-7.76 (7H, H^g (3S₄, 4C₃)), 7.96 (1H, d, *J* = 4.91 Hz, H^g (T)), 7.96-7.34 (14H, H^a (3S₄, 4C₃)), 7.65 (2H, d, *J* = 8.21 Hz, H^a (T)), 5.93-5.40 (14H, H^b (3S₄, 4C₃)), 5.69 (2H, d, *J* = 8.31 Hz, H^b (T)). ¹⁹F NMR (376 MHz; 298 K; CD₃CN): δ -64.69 (d, *J* = 718.33 Hz, [PF₆⁻1-S₄]), -64.92 (d, *J* = 716.91 Hz, [PF₆⁻1-T]), -65.40 (d, *J* = 717.61 Hz, [PF₆⁻1-C₃]), -73.75 (d, *J* = 706.59, PF₆⁻). *m/z* (ESI-MS) = 363.25 [**1** + PF₆⁻]⁷⁺.

Elemental Analysis (%) calcd for $C_{144}H_{108}F_{48}Fe_4N_{24}P_8 \cdot 3H_2O$: C, 47.89%; H, 3.18%; N, 9.31%. Found: C, 47.88%; H, 3.18%; N, 9.23%.

1.2.4 $[ClO_4 \subset 1] \cdot 7ClO_4 \cdot 12H_2O$.

Yield 307 mg, 84 %. 1H NMR (400 MHz; 298 K; CD_3CN): δ 9.00 (2H, s, H^c ($2S_4$)), 8.83 (1H, s, H^c (S_4)), 8.79 (2H, s, H^c ($2C_3$)), 8.75 (1H, s, H^c (C_3)), 8.72 (1H, s, H^c (T)), 8.72 (1H, s, H^c (C_3)), 8.56-8.30 (14H, H^d ($3S_4$, $4C_3$) and H^e ($3S_4$, $4C_3$)), 8.40 (1H, d, $J = 7.38$ Hz, H^d (T)), 8.34 (1H, t, $J = 7.65$ Hz, H^e (T)), 8.06-7.59 (21H, H^a ($3S_4$, $4C_3$) and H^f ($3S_4$, $4C_3$)), 7.81 (2H, d, $J = 7.97$ Hz, H^a (T)), 7.73 (1H, t, $J = 6.61$ Hz, H^f (T)), 7.54-7.27 (7H, H^g ($3S_4$, $4C_3$)), 7.44 (1H, d, $J = 5.31$ Hz, H^g (T)), 5.95-5.30 (14H, H^b ($3S_4$, $4C_3$)), 5.54 (2H, d, $J = 8.44$ Hz, H^b (T)). m/z (ESI-MS) = 356.77 [$1 + ClO_4^-$] $^{7+}$. Elemental Analysis (%) calcd for $C_{144}H_{108}Cl_8Fe_4N_{24}O_{32} \cdot 12H_2O$: C, 50.72%; H, 3.90%; N, 9.86%. Found: C, 50.34 %; H, 3.36%; N, 9.63%.

1.2.5 $[BF_4 \subset 1] \cdot 7BF_4 \cdot 3MeCN$.

Yield 289 mg, 80 %. 1H NMR (400 MHz; 298 K; CD_3CN): δ 8.68 (1H, s, H^c), 8.39 (1H, d, $J = 7.33$ Hz, H^d), 8.34 (1H, t, $J = 7.29$ Hz, H^e), 7.78 (2H, d, H^a), 7.72 (1H, t, $J = 6.53$ Hz, H^f), 7.41 (1H, d, $J = 4.91$ Hz, H^g), 5.46 (2H, d, $J = 7.76$ Hz, H^b). ^{19}F NMR (376 MHz; 298 K; CD_3CN): δ -141.30 (s, (^{10}B) [$BF_4 \subset 1$]), -141.35 (s, (^{11}B) [$BF_4 \subset 1$]), -151.00 (s, (^{10}B) [$BF_4 \subset 1$]), -151.05 (s, (^{11}B) [$BF_4 \subset 1$]). m/z (ESI-MS) = 354.8 [$1 + BF_4^-$] $^{7+}$. Elemental Analysis (%) calcd for $C_{144}H_{108}B_8F_{32}Fe_4N_{24} \cdot 3MeCN$: C, 56.02%; H, 3.67%; N, 11.76%. Found: C, 56.37 %; H, 2.81%; N, 11.66%.

1.3 Additional characterization details

1.3.1 X-ray structure of Hexakis(acetonitrile)iron(II) hexafluorophosphate

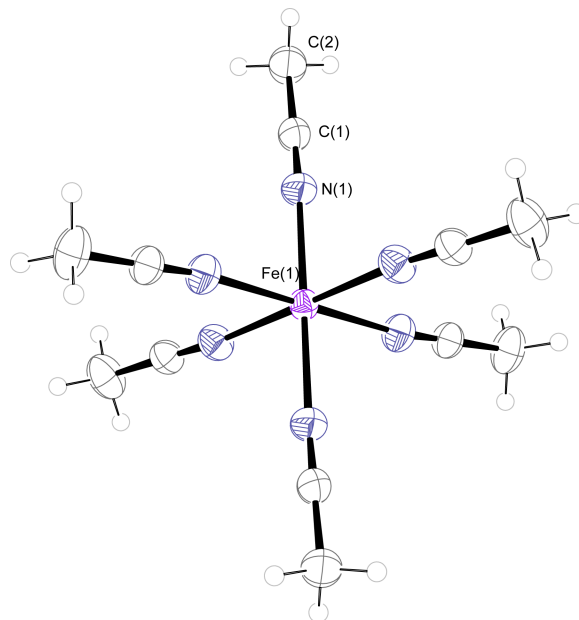


Figure S1: ORTEP representation of the cation in the crystal structure of $[\text{Fe}(\text{MeCN})_6] \cdot 2\text{PF}_6$ shown with 50 % probability ellipsoids.

1.3.2 Additional characterization for $[1] \cdot 8NTf_2$

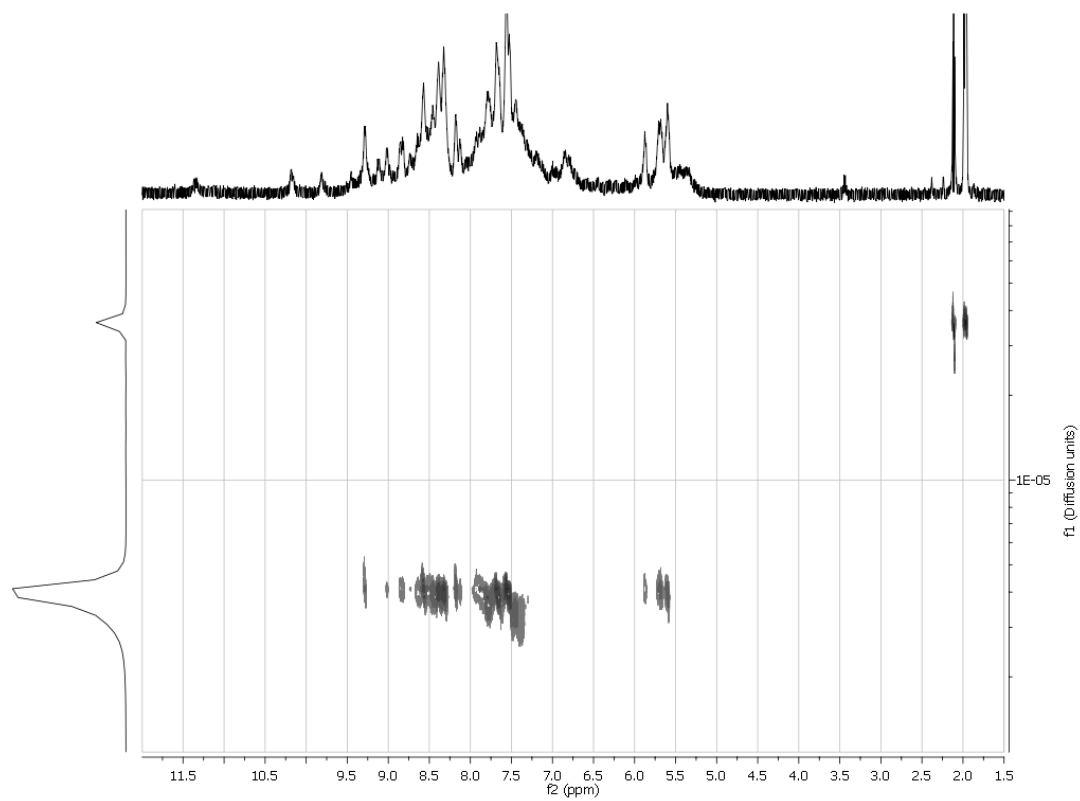


Figure S2: ^1H DOSY (500 MHz, CD_3CN) for $[1] \cdot 8\text{NTf}_2$

Table S1: Guests trialed for 1^{8+} .

Guest		Guest	
PF₆⁻	Encapsulation	I⁻	Encapsulation
ClO₄⁻	Encapsulation	SiF₆²⁻	No encapsulation
BF₄⁻	Encapsulation	SiF₅⁻	No encapsulation
Benzene	No encapsulation	THF	No encapsulation
Cyclopentane	No encapsulation	NO₃⁻	Encapsulation
CCl₄	No encapsulation	OCN⁻	Decomposition
CH₂Cl₂	No encapsulation	SO₃NH₂⁻	No encapsulation
SO₄²⁻	Decomposition	Acetate	Decomposition
H₂PO₄⁻	Decomposition	Iodoform	No encapsulation
CO₂	No encapsulation	Bromoform	No encapsulation
Cl⁻	Encapsulation	SnI₄	No encapsulation
Br⁻	Encapsulation	F⁻	Decomposition
AsF₆⁻	Encapsulation	SbF₆⁻	No encapsulation
MnO₄⁻	Decomposition	IO₄⁻	Decomposition
HPO₄²⁻	Decomposition	PO₄³⁻	Decomposition
HSO₄⁻	No encapsulation	Chloroform	No encapsulation

1.3.3 Additional characterization for $[\text{BF}_4\text{C1}]\cdot 7\text{BF}_4$

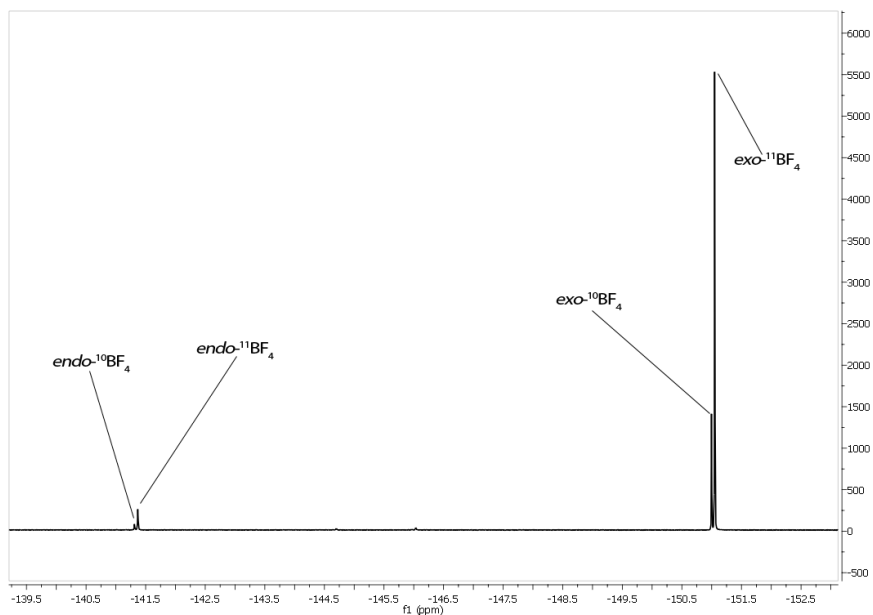


Figure S3: ^{19}F NMR (376 MHz, CD_3CN) for $[\text{BF}_4\text{C1}]\cdot 7\text{BF}_4$

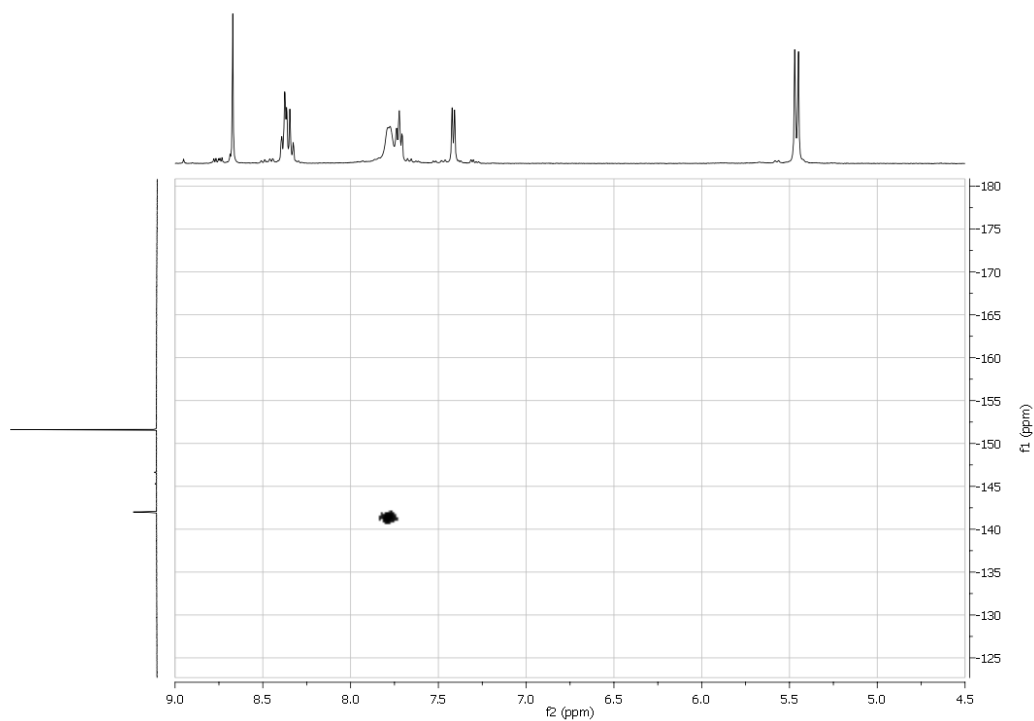


Figure S4: ^{19}F - ^1H HOESY NMR for $[\text{BF}_4\text{C1}]\cdot 7\text{BF}_4$

1.3.4 Additional characterization for $[\text{PF}_6\text{C}1]\cdot 7\text{PF}_6$

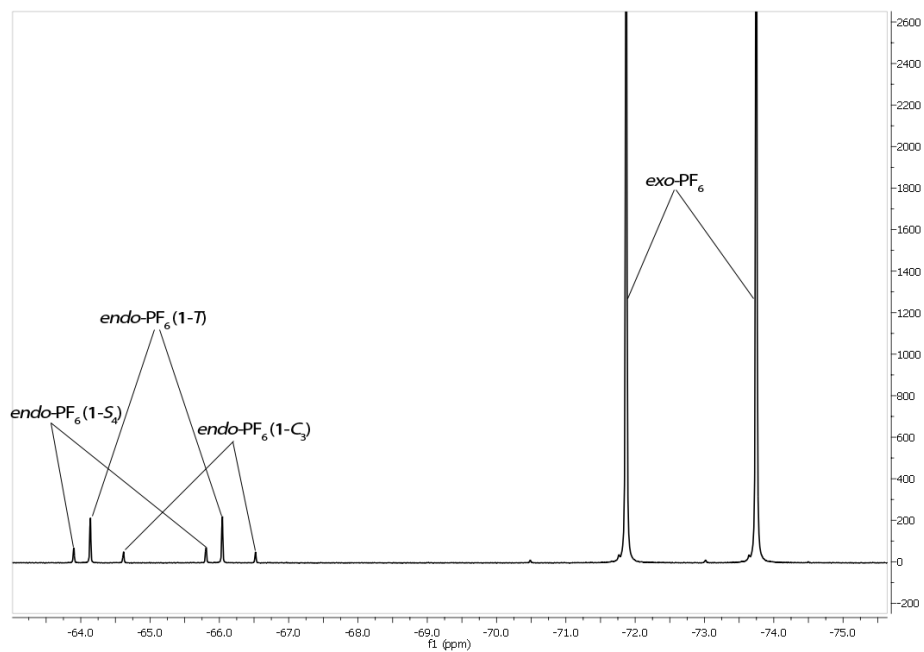


Figure S5: ^{19}F NMR (376 MHz, CD_3CN) for $[\text{PF}_6\text{C}1]\cdot 7\text{PF}_6$

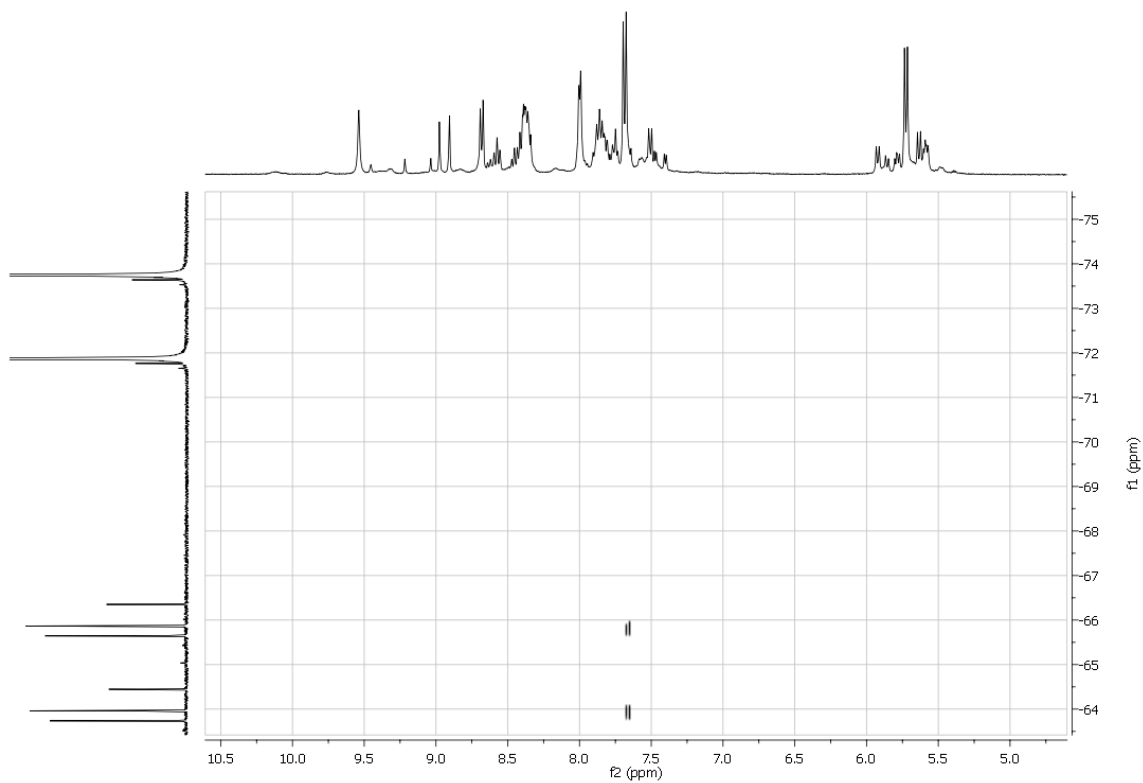


Figure S6: ^{19}F - ^1H HOESY NMR for $[\text{PF}_6\text{C}1]\cdot 7\text{PF}_6$

1.4 Crystallography

Data were collected either using a Nonius Kappa FR590 diffractometer employing graphite-monochromated Mo-K α radiation generated from a sealed tube (0.71073 Å) with ω and ψ scans at 180(2) K;^{S4} an Oxford Gemini Ultra employing confocal mirror monochromated Cu-K α radiation generated from a sealed tube (1.5418 Å) with ω and ψ scans at 120(2) K;^{S5} a Nonius Kappa FR591 diffractometer employing confocal mirror-monochromated Mo-K α radiation generated from a rotating anode (0.71073 Å) with ω and ψ scans at 120(2) K^{S4}; or at Beamline I19 of Diamond Light Source employing silicon double crystal monochromated synchrotron radiation (0.6889 Å) with ω scans at 100(2) K.^{S6} Data integration and reduction were undertaken with S HKL Denzo and Scalepack,^{S4, 7} CrysAlisPro^{S5} or CrystalClear^{S6} respectively. Subsequent computations were carried out using the WinGX-32 graphical user interface.^{S8} Multi-scan empirical absorption corrections were applied to the data using the programs SADABS,^{S9} SORTAV,^{S10} CrysAlisPro^{S5} or CrystalClear.^{S6} Gaussian absorption corrections were applied using CryAlisPro.^{S5} Structures were solved by direct methods using SIR97^{S11} or charge-flipping with SUPERFLIP^{S12} then refined and extended with SHELXL-97 or SHELXH-97.^{S13} In general, non-hydrogen atoms with occupancies greater than 0.5 were refined anisotropically. Carbon-bound hydrogen atoms were included in idealized positions and refined using a riding model. Crystallographic data along with specific details pertaining to the refinement (inclusively addressing CheckCIF alerts), where required, follow.

1.4.1 [Fe(MeCN)₆] \cdot 2PF₆

Crystals were grown by the slow diffusion of diethyl ether into an acetonitrile solution of the product.

Formula C₁₂H₁₈F₁₂FeN₆P₂, M 592.11, Trigonal, space group $R\bar{3}(\#148)$, a 11.2049(16), b 11.2049(16), c 16.640(3) Å, γ 120.00°, V 1809.2(5) Å³, D_c 1.630 g cm⁻³, Z 3, crystal size 0.23 by 0.23 by 0.23 mm, colour colourless, habit block, temperature 180(2) Kelvin, $\lambda(\text{MoK}\alpha)$ 0.71073 Å, $\mu(\text{MoK}\alpha)$ 0.861 mm⁻¹, T(SORTAV)_{min,max} 0.766, 0.826, $2\theta_{\text{max}}$ 56.52, hkl range -14 14, -14 14, -22 21, N 8042, N_{ind} 997(R_{merge} 0.0289), N_{obs} 902($I > 2\sigma(I)$), N_{var} 52, residuals* $R1(F)$ 0.0756, $wR2(F^2)$ 0.2361, GoF(all) 1.102, $\Delta\rho_{\text{min,max}}$ -0.538, 1.711 e⁻ Å⁻³.

* $R1 = \sum||F_o| - |F_c||/\sum|F_o|$ for $F_o > 2\sigma(F_o)$; $wR2 = (\sum w(F_o^2 - F_c^2)^2/\sum(wF_c^2)^2)^{1/2}$ all reflections

$w=1/[\sigma^2(F_o^2)+(0.17520P)^2+3.6873P]$ where $P=(F_o^2+2F_c^2)/3$

1.4.2 [I \bar{C} -I] \cdot 3I \cdot 3.5OTf \cdot 0.5NTf₂ \cdot 2MeCN \cdot Et₂O

Crystals were grown by the slow diffusion of diethyl ether into an acetonitrile solution of **1·8OTf** to which had been added 10 equivalents of tetrabutylammonium iodide and 10 equivalents of tetrabutylammonium triflimide. This data was collected at the Diamond Light Source.

Specific details: The crystals employed rapidly lost solvent after removal from the mother liquor. Rapid (<1 min) handling at dry ice temperatures prior to quenching in the cryostream was required to collect data. A number of the anions in the structure are disordered and were modelled with partial occupancies and rigid-body constraints. In addition, reflecting the instability of the crystals, there is a large area of smeared electron density present in the lattice. Despite many attempts to model this region of disorder as a combination of solvent and anion molecules no reasonable fit could be found and accordingly this region was treated with the SQUEEZE^{S14} function of PLATON.^{S15}

Formula C₁₅₆H₁₂₄F₁₂Fe₄I₄N_{26.50}O₁₂S₄, M 3649.06, monoclinic, space group C2/c(#15), a 34.740(13), b 18.276(7), c 53.69(2) Å, β 95.757(5), V 33916(22) Å³, D_c 1.429 g cm⁻³, Z 8, crystal size 0.01 by 0.01 by 0.01 mm, colour purple, habit needle, temperature 100(2) Kelvin, λ(Synchrotron) 0.68890 Å, μ(Synchrotron) 1.189 mm⁻¹, T(CRYSTALCLEAR)_{min,max} 0.782, 1.000, 2θ_{max} 49.48, hkl range -41 41, -21 21, -55 64, N 134487, N_{ind} 30645 (R_{merge} 0.0799), N_{obs} 23498 (I > 2σ(I)), N_{var} 1723, residuals* R1(F) 0.1008, wR2(F²) 0.2946, GoF(all) 1.229, Δρ_{min,max} -1.658, 3.123 e⁻ Å⁻³.

*R1 = Σ||F_o| - |F_c||/Σ|F_o| for F_o > 2σ(F_o); wR2 = (Σw(F_o² - F_c²)/Σ(wF_c²))^{1/2} all reflections
w=1/[σ²(F_o²)+(0.2000P)²+0.0000P] where P=(F_o²+2F_c²)/3

1.4.3 [I-S₄]·8NTf₂·5MeCN·2H₂O·Et₂O

The crystal was grown by the slow diffusion of diethyl ether into an acetonitrile solution of **1·8NTf₂**.

Specific details: The crystals employed rapidly lost solvent after removal from the mother liquor. Rapid (<1 min) handling at dry ice temperatures prior to quenching in the cryostream was required to collect data. A number of the anions in the structure are disordered and were modelled with multiple sulfur positions, in addition the anions exhibit larger than ideal thermal parameters and U_{eq} max/min ratios due to thermal motion and unresolved disorder. Consequently, a number of constraints and restraints were required to facilitate realistic modelling. The water hydrogen atoms could not be located and were not modelled.

Formula C₁₇₄H₁₃₇F₄₈Fe₄N₃₇O₃₅S₁₆, M 4954.57, monoclinic, space group P2/c(#13), a 20.2319(5), b 19.1597(5), c 29.2305(9) Å, β 102.582(3), V 11058.7(5) Å³, D_c 1.488 g cm⁻³, Z 2, crystal size 0.6264 by 0.4515 by 0.3531 mm, colour purple, habit blade, temperature 120(2) Kelvin, λ(CuKα) 1.54184 Å, μ(CuKα) 4.489 mm⁻¹,

$T(\text{Analytical})_{\text{min,max}}$ 0.060, 0.355, $2\theta_{\text{max}}$ 143.86, hkl range -20 24, -22 10, -35 26, N 46353, N_{ind} 21093 (R_{merge} 0.0555), N_{obs} 16628 ($I > 2\sigma(I)$), N_{var} 1426, residuals* $R1(F)$ 0.1365, $wR2(F^2)$ 0.3237, $\text{GoF}(\text{all})$ 1.361, $\Delta\rho_{\text{min,max}}$ -1.194, 1.933 $\text{e}^- \text{\AA}^{-3}$.

* $R1 = \Sigma||F_o| - |F_c||/\Sigma|F_o|$ for $F_o > 2\sigma(F_o)$; $wR2 = (\Sigma w(F_o^2 - F_c^2)^2/\Sigma(wF_c^2)^2)^{1/2}$ all reflections

$w=1/[\sigma^2(F_o^2)+(0.1000P)^2+45.0000P]$ where $P=(F_o^2+2F_c^2)/3$

1.4.4 [PF₆Cl-T]·7PF₆·9MeCN·3Et₂O

Crystals were grown by the slow diffusion of diethyl ether to an acetonitrile solution of 1·8PF₆ to which had been added 100 equivalents of tetrabutylammonium hexafluorophosphate.

Specific details: While appearing of good quality and despite rapid handling at low temperature, the use of a cryostream and long exposure times no reflection data could be observed at better than 1.0 Å resolution. Nevertheless, the data is of more than sufficient quality to unambiguously establish the connectivity of the structure. Each of the anions and a number of the solvent molecules required a number of bond length constraints to facilitate realistic modelling and a number have larger than ideal thermal parameters reflecting unresolved thermal motion. In addition, reflecting the instability of the crystals, there is a large area of smeared electron density present in the lattice. Despite many attempts to model this region of disorder as a combination of solvent and anion molecules no reasonable fit could be found and accordingly this region was treated with the SQUEEZE^{S14} function of PLATON.^{S15}

Formula C₁₇₄H₂₀₄F₄₈Fe₄N₃₃O₃P₈, M 4188.86, orthorhombic, space group $Pna2_1$ (#33), a 34.2735(5), b 32.0208(9), c 18.4925(3) Å, V 20294.9(7) Å³, D_c 1.371 g cm⁻³, Z 4, crystal size 0.20 by 0.15 by 0.05 mm, colour purple, habit needle, temperature 150(2) Kelvin, $\lambda(\text{CuK}\alpha)$ 1.54184 Å, $\mu(\text{CuK}\alpha)$ 3.732 mm⁻¹, $T(\text{CRYALISPRO})_{\text{min,max}}$ 0.17261, 1.00000, $2\theta_{\text{max}}$ 102.42, hkl range -34 34, -31 32, -18 15, N 45610, N_{ind} 17903 (R_{merge} 0.0371), N_{obs} 14119 ($I > 2\sigma(I)$), N_{var} 1905, residuals* $R1(F)$ 0.0940, $wR2(F^2)$ 0.2552, $\text{GoF}(\text{all})$ 1.074, $\Delta\rho_{\text{min,max}}$ -0.882, 1.172 $\text{e}^- \text{\AA}^{-3}$.

* $R1 = \Sigma||F_o| - |F_c||/\Sigma|F_o|$ for $F_o > 2\sigma(F_o)$; $wR2 = (\Sigma w(F_o^2 - F_c^2)^2/\Sigma(wF_c^2)^2)^{1/2}$ all reflections

$w=1/[\sigma^2(F_o^2)+(0.1995P)^2+9.6169P]$ where $P=(F_o^2+2F_c^2)/3$

1.4.5 [ClO₄Cl-T]·4ClO₄·3OTf·4MeCN·2Et₂O

These crystals were grown by the slow diffusion of diethyl ether into an acetonitrile solution of 1·8OTf to which had been added 10 equivalents of tetrabutylammonium perchlorate. This data was collected by the EPSRC National Crystallographic Service.^{S16}

Specific details: The crystals rapidly lost solvent after removal from the mother liquor. Rapid (<1 min) handling at dry ice temperatures prior to quenching in the cryostream was required to collect data. Some of the anions display high thermal motion indicating unresolved disorder and a number of bond length constraints were required to facilitate realistic modelling. In addition, reflecting the instability of the crystals, there is a large area of smeared electron density present in the lattice. Despite many attempts to model this region of disorder as a combination of solvent and anion molecules no reasonable fit could be found and accordingly this region was treated with the SQUEEZE^{S14} function of PLATON.^{S15}

Formula C₁₆₃H₁₃₀Cl₅F₉Fe₄N₂₈O₃₀S₃, M 3628.78, monoclinic, space group C2/c(#15), a 34.8667(8), b 18.4699(4), c 54.2074(11) Å, β 96.3680(10), V 34693.3(13) Å³, D_c 1.389 g cm⁻³, Z 8, crystal size 0.21 by 0.18 by 0.11 mm, colour purple, habit block, temperature 120(2) Kelvin, λ(MoKα) 0.71073 Å, μ(MoKα) 0.528 mm⁻¹, T(SADABS)_{min,max} 0.772986, 1.000, 2θ_{max} 46.52, hkl range -38 38, -20 20, -59 60, N 116008, N_{ind} 24758 (R_{merge} 0.0729), N_{obs} 16013 (I > 2σ(I)), N_{var} 1969, residuals * R1(F) 0.1071, wR2(F²) 0.3185, GoF(all) 1.081, Δρ_{min,max} -1.123, 1.895 e⁻ Å⁻³.

*R1 = Σ||F_o| - |F_c||/Σ|F_o| for F_o > 2σ(F_o); wR2 = (Σw(F_o² - F_c²)/Σ(wF_c²))^{1/2} all reflections

w=1/[σ²(F_o²)+(0.1896P)²+140.4826P] where P=(F_o²+2F_c²)/3

1.4.6 [BF₄Cl-T]·7BF₄·5.25MeCN·0.25Et₂O

These crystals were grown by the slow diffusion of diethyl ether into an acetonitrile solution of [1]·8ClO₄. This data was collected by the EPSRC National Crystallographic Service.^{S16}

Specific details: This structure has an extremely large unit cell with two full cage molecules per asymmetric unit. While appearing of good quality and despite rapid handling at low temperature, the use of a cryostream and long exposure times no reflection data was observed at better than 1.1 Å resolution. In addition, the crystal employed in this study proved to be twinned by a two-fold rotation about -1 0 0. As a consequence the data is of less than ideal quality, but nevertheless more than suitable for unambiguously establishing the connectivity of the structure. Due to the limitations of the data, each six membered ring was modelled as a rigid body with each set of atoms in the ring with identical thermal parameters. Each of the anions also required both constraints and restraints to facilitate realistic modelling. Not all of the anions could be located in the difference Fourier map and as a result residual peaks were included as partial occupancy fluorine atoms until a plateau of 1.5 e⁻ Å⁻³ was reached. Collectively due to the above, the residuals of the structure are poor.

Formula C_{155.50}H_{125.875}B₈F₃₂Fe₄N_{29.25}O_{0.25}, M 3326.11, monoclinic, space group P2₁/c(#14), a 18.1572(15), b 56.898(6), c 36.253(4) Å, β 96.002(4), V 37248(6) Å³, D_c 1.186 g cm⁻³, Z 8, crystal size 0.38 by 0.16 by 0.04 mm, colour purple, habit lath,

temperature 120(2) Kelvin, $\lambda(\text{MoK}\alpha)$ 0.71073 Å, $\mu(\text{MoK}\alpha)$ 0.389 mm⁻¹, $T(\text{TWINABS})_{\text{min,max}}$ 0.088354, 1.0000, $2\theta_{\text{max}}$ 37.70, hkl range -16 16, 0 51, 0 32, N 31098, N_{obs} 23760 ($I > 2\sigma(I)$), N_{var} 1564, residuals* $R1(F)$ 0.2209, $wR2(F^2)$ 0.5161, $\text{GoF}(\text{all})$ 1.136, $\Delta\rho_{\text{min,max}}$ -1.023, 1.574 e⁻ Å⁻³.

* $R1 = \Sigma||F_o| - |F_c||/\Sigma|F_o|$ for $F_o > 2\sigma(F_o)$; $wR2 = (\Sigma w(F_o^2 - F_c^2)^2/\Sigma(wF_c^2)^2)^{1/2}$ all reflections

$w=1/[\sigma^2(F_o^2)+(0.0850P)^2+1891.2368P]$ where $P=(F_o^2+2F_c^2)/3$

1.5 Titrations

1.5.1 Method for direct titration

A stock solution (10 mL) of **1**·8NTf₂ with a concentration of 7.8×10⁻⁴ M was prepared in CD₃CN. 500 μL were transferred to a J-Young NMR tube. The remaining stock solution was split into four and to each of these approximately 10 eq. of the selected guest were added as the appropriate tetrabutylammonium or tetramethylammonium salt. This procedure ensures that the concentration of host **1**·8NTf₂ was kept constant throughout the titration experiment. Small aliquots of the guest solution were titrated into the J-Young NMR tube. The solution was allowed to equilibrate at 50 °C overnight and was left to cool to room temperature for 30 minutes before acquiring the ¹H NMR spectrum. Data were then fitted using the model derived below.

1.5.2 Method for the competitive displacement of PF₆ by bromide.

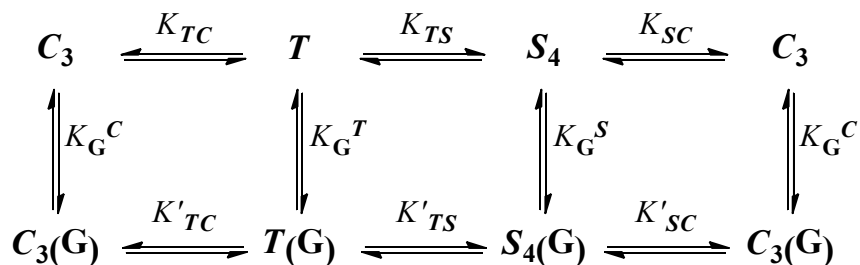
A stock solution (5 mL) of **1**·8NTf₂ with a concentration of 7.8×10⁻⁴ M was prepared in CD₃CN. 100 equivalents tetrabutylammonium hexafluorophosphate were added to the solution. 500 μL was transferred to a J-Young NMR tube. To the remaining stock solution were added 4 equivalents (relative to total host) of tetrabutylammonium bromide. This procedure ensures that the concentration of host **1**·8NTf₂ was kept constant throughout the titration experiment. Small aliquots of the guest solution were titrated into the J-Young NMR tube. The solution was allowed to equilibrate at 50 °C overnight and was left to cool to room temperature for 30 minutes before acquiring the ¹⁹F NMR spectrum. Data were then fitted using an established competitive binding model.^{S17}

1.5.3 Method for relative binding investigations

A stock solution (10 mL) of **1**·8BF₄ with a concentration of 7.8×10⁻⁴ M was prepared in CD₃CN. To 400 μL aliquots of this solution were added 1 equivalent of the appropriate tetrabutylammonium or tetramethylammonium salt in CD₃CN. The solution was allowed to equilibrate at 50 °C overnight and was left to cool to room temperature for 30 minutes before acquiring the ¹H NMR spectrum. Each measurement was repeated three times and the relative integrals of the host-guest complexes averaged (error ~10 %).^{S18}

1.5.4 Derivation of binding model guest encapsulation in the system of 1.

Consider three diastereomeric cages with T , S_4 and C_3 symmetry, which are in equilibrium with each other. Also each of three diastereomers can encapsulate a guest G , leading to the three filled diastereomeric cages, $T(G)$, $S_4(G)$ and $C_3(G)$, which are also in equilibrium with each other. Scheme S1 shows the different equilibria and related equilibrium constants.



Scheme S1: Overview of the relevant equilibria and corresponding equilibrium constants.

Let us define first all the equilibrium constants:

$$K_{TC} = [C_3] / [T] \quad (1)$$

$$K_{TS} = [S_4] / [T] \quad (2)$$

$$K_{SC} = [C_3] / [S_4] = K_{TC} / K_{TS} \quad (3)$$

$$K'_{TC} = [C_3(G)] / [T(G)] \quad (4)$$

$$K'_{TS} = [S_4(G)] / [T(G)] \quad (5)$$

$$K'_{SC} = [C_3(G)] / [S_4(G)] = K'_{TC} / K'_{TS} \quad (6)$$

$$K_G^T = [T(G)] / ([T] \times [G]) \quad (7)$$

$$K_G^S = [S_4(G)] / ([S_4] \times [G]) \quad (8)$$

$$K_G^C = [C_3(G)] / ([C_3] \times [G]) \quad (9)$$

Starting with the mass balance for the total host concentration, $[H]_0$:

$$[H]_0 = [T] + [S_4] + [C_3] + [T(G)] + [S_4(G)] + [C_3(G)] \quad (10)$$

$$= [T] \times (1 + K_{TS} + K_{TC}) + [T(G)] \times (1 + K'_{TS} + K'_{TC})$$

Let's define the following two parameters:

$$p = 1 + K_{TS} + K_{TC} \quad (11)$$

$$q = 1 + K'_{TS} + K'_{TC} \quad (12)$$

Now equation 10 can be rewritten as:

$$[H]_0 = p \times [T] + q \times [T(G)] \quad (13)$$

From equation 7 we can express $[T]$ as:

$$[T] = [T(G)] / (K_G^T \times [G]) \quad (14)$$

Inserting equation 14 in equation 13 yields:

$$[H]_0 = p \times [T(G)] / (K_G^T \times [G]) + q \times [T(G)] \quad (15)$$

Let's now consider the mass balance for the total guest concentration, $[G]_0$:

$$\begin{aligned} [G]_0 &= [G] + [T(G)] + [S_4(G)] + [C_3(G)] \\ &= [G] + [T(G)] \times (1 + K'_{TS} + K'_{TC}) \\ &= [G] + q \times [T(G)] \end{aligned} \quad (16)$$

Rearranging equation 16, gives the expression for the free guest concentration, $[G]$:

$$[G] = [G]_0 - q \times [T(G)] \quad (17)$$

Before inserting equation 17 into equation 15, equation 15 is rearranged to:

$$[H]_0 \times [G] = (p / K_G^T) \times [T(G)] + q \times [T(G)] \times [G] \quad (18)$$

Now we can insert equation 17 into equation 18, which leads to:

$$[H]_0 \times ([G]_0 - q \times [T(G)]) = (p / K_G^T) \times [T(G)] + q \times [T(G)] \times ([G]_0 - q \times [T(G)]) \quad (19)$$

Rewriting equation 19 gives:

$$[H]_0 \times [G]_0 - q \times [H]_0 \times [T(G)] = (p / K_G^T) \times [T(G)] + q \times [G]_0 \times [T(G)] - q^2 \times [T(G)]^2 \quad (20)$$

Which is identical to:

$$q^2 \times [T(G)]^2 - (q \times [H]_0 + (p / K_G^T) + q \times [G]_0) \times [T(G)] + [H]_0 \times [G]_0 = 0 \quad (21)$$

Equation 21 is a quadratic equation in $[T(G)]$, having the following A, B and C parameters:

$$A = q^2 \quad (22)$$

$$B = -(q \times [H]_0 + (p / K_G^T) + q \times [G]_0)$$

$$C = [H]_0 \times [G]_0$$

The general solution of the quadratic equation is equal to:

$$[TG] = \frac{-B \pm \sqrt{B^2 - 4AC}}{2A} \quad (23)$$

Inserting the values for A, B and C, gives:

$$[TG] = \frac{\left(q \times [H]_0 + \frac{p}{K_G^T} + q \times [G]_0\right) \pm \sqrt{\left(q \times [H]_0 + \frac{p}{K_G^T} + q \times [G]_0\right)^2 - 4 \times q^2 \times [H]_0 \times [G]_0}}{2q^2} \quad (24)$$

From the two general solutions given above, the physical relevant root is given by:

$$[TG] = \frac{\left(q \times [H]_0 + \frac{p}{K_G^T} + q \times [G]_0\right) - \sqrt{\left(q \times [H]_0 + \frac{p}{K_G^T} + q \times [G]_0\right)^2 - 4 \times q^2 \times [H]_0 \times [G]_0}}{2q^2} \quad (25)$$

Plotting $[T(G)]$ as a function of $[G]_0$, allows for the determination of K_G^T , provided that the constants p , q and $[H]_0$ are known. p and q can be determined from the NMR. Knowing K_G^T , it is possible to also determine the binding constants K_G^S and K_G^C , since it holds that:

$$K_G^S = [S_4(G)] / ([S_4] \times [G]) = ([T] / [S_4]) \times ([T(G)] / ([T] \times [G])) \times (S_4(G) / [T(G)]) \quad (26)$$
$$= 1/K_{TS} \times K_G^T \times K'_{TS} = (K'_{TS} / K_{TS}) \times K_G^T$$

Similarly, for K_G^C it holds:

$$K_G^C = (K'_{TC} / K_{TC}) \times K_G^T \quad (27)$$

1.5.5 Curves obtained for direct titration of Γ , BF_4^- and ClO_4^- , each showing strong binding.

As each of these anions were such strong binders it was not possible to obtain an accurate K_a value from the data. Simulations of different K_a values was made to show that the binding constant has a lower limit of $1 \times 10^6 \text{ M}^{-1}$. In each figure squares represent experimental data and coloured lines represent simulated binding curves.

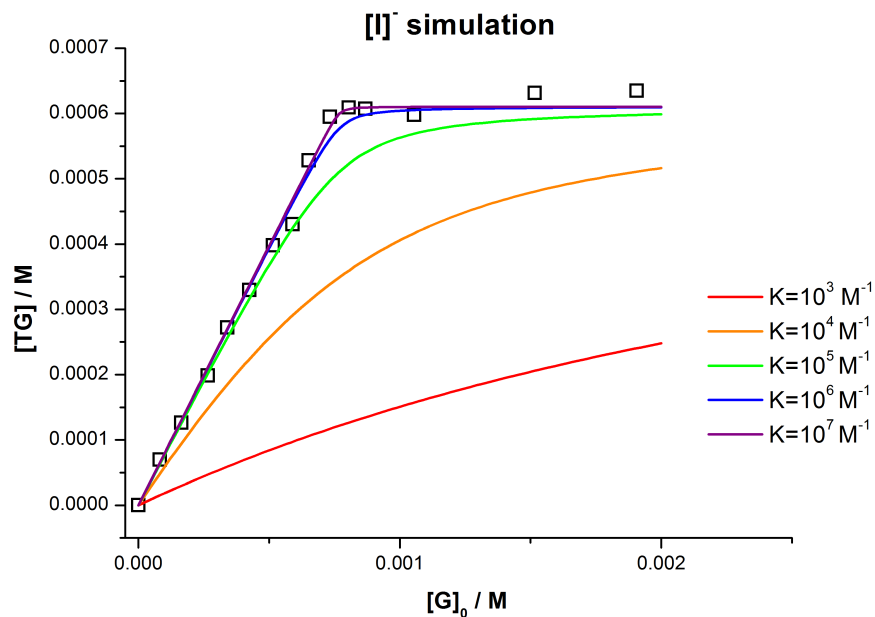


Figure S7: Simulation of the Γ^- binding curve showing that K_a has a lower limit of $1 \times 10^6 \text{ M}^{-1}$

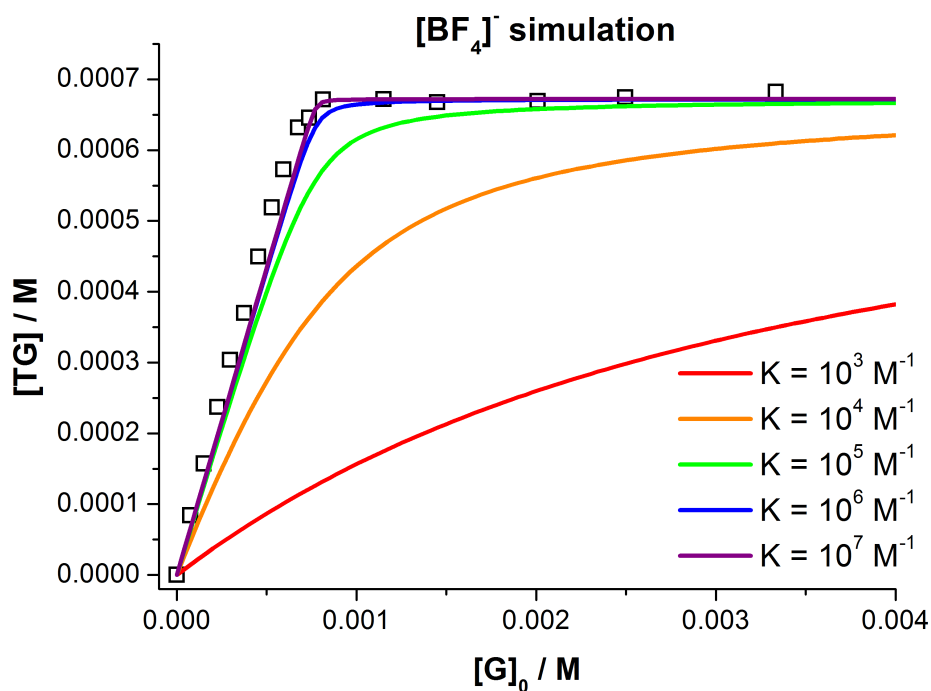


Figure S8: Simulation of the BF₄⁻ binding curve showing that K_a has a lower limit of $1 \times 10^6 \text{ M}^{-1}$

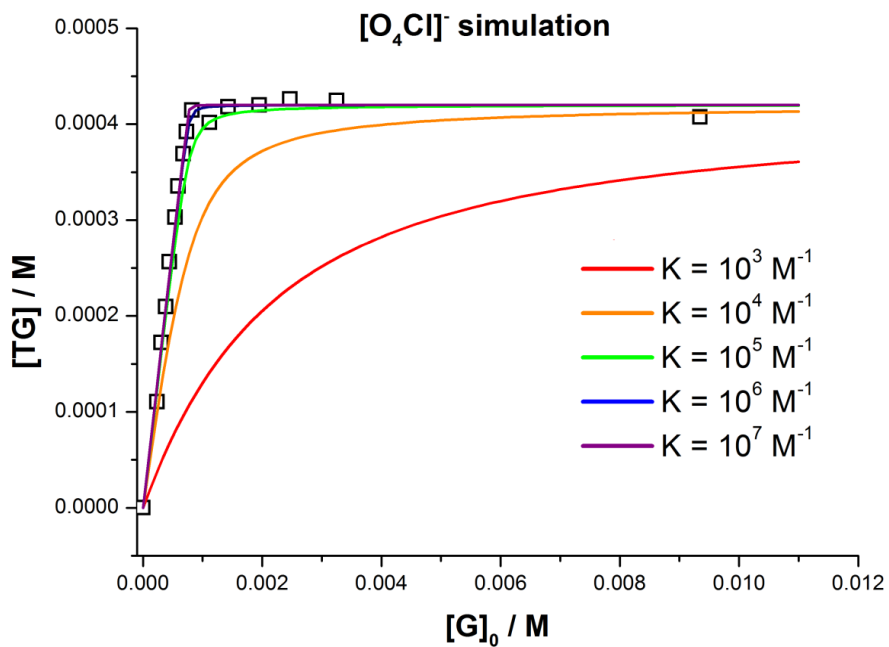


Figure S9: Simulation of the ClO₄⁻ binding curve showing that K_a has a lower limit of $1 \times 10^6 \text{ M}^{-1}$

1.5.6 Data fitting for direct titration of PF_6^- into I^{8+} .

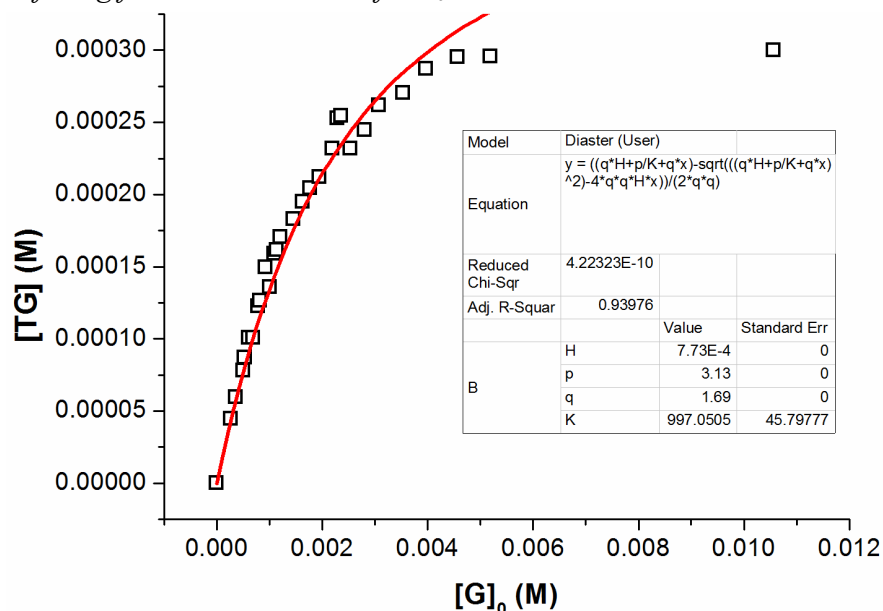


Figure S10: Data fitting for the titration of PF_6^- into I^{8+}

1.5.7 Data fitting for competitive titration of Br^- against PF_6^- .

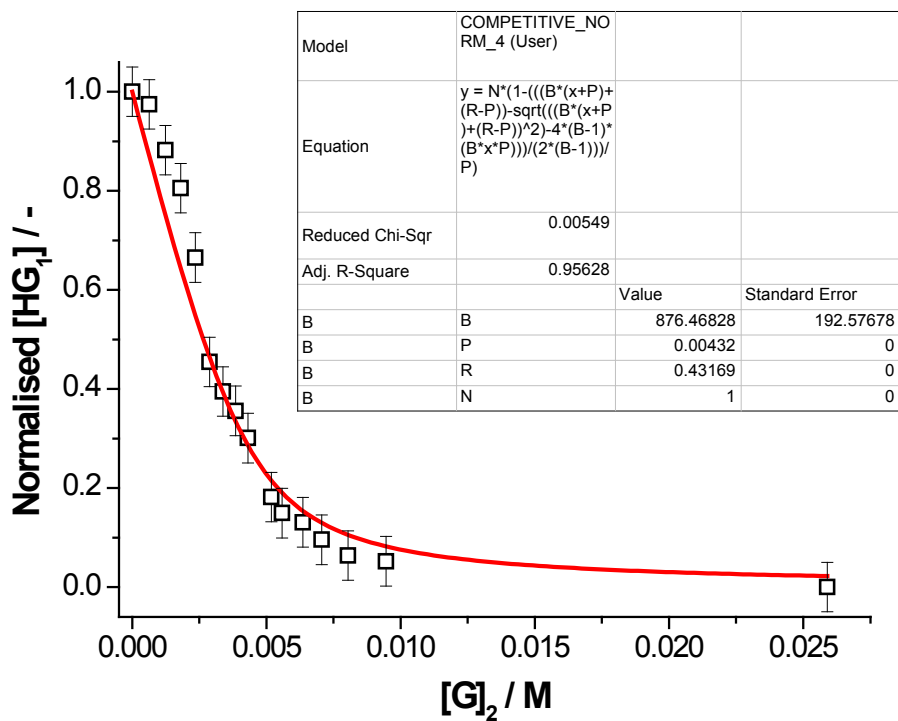


Figure S11: Data fitting for displacement of PF_6^- by Br^-

1.6 Molecular Modelling and Anion Volume Calculations.

These calculations were performed using SPARTAN '10.^{S19} Molecular Modelling calculations were performed at the PM3 level, while anion volumes were calculated at MP2 with a 6-311+G** basis set. The atomic coordinates were taken from the crystal structure of $[\text{PF}_6\text{C}\mathbf{1}]\cdot 7\text{PF}_6$ and metal-ligand bonds and angles were fixed as they were determined crystallographically. Constraints were then placed on the corresponding φ angles to maintain approximate *T*-symmetry and PM3 equilibrium geometry calculations performed at every 10 degrees between $-90 \leq \varphi \leq 90$. The resulting structures were then used in for volume calculations. Results are shown below.

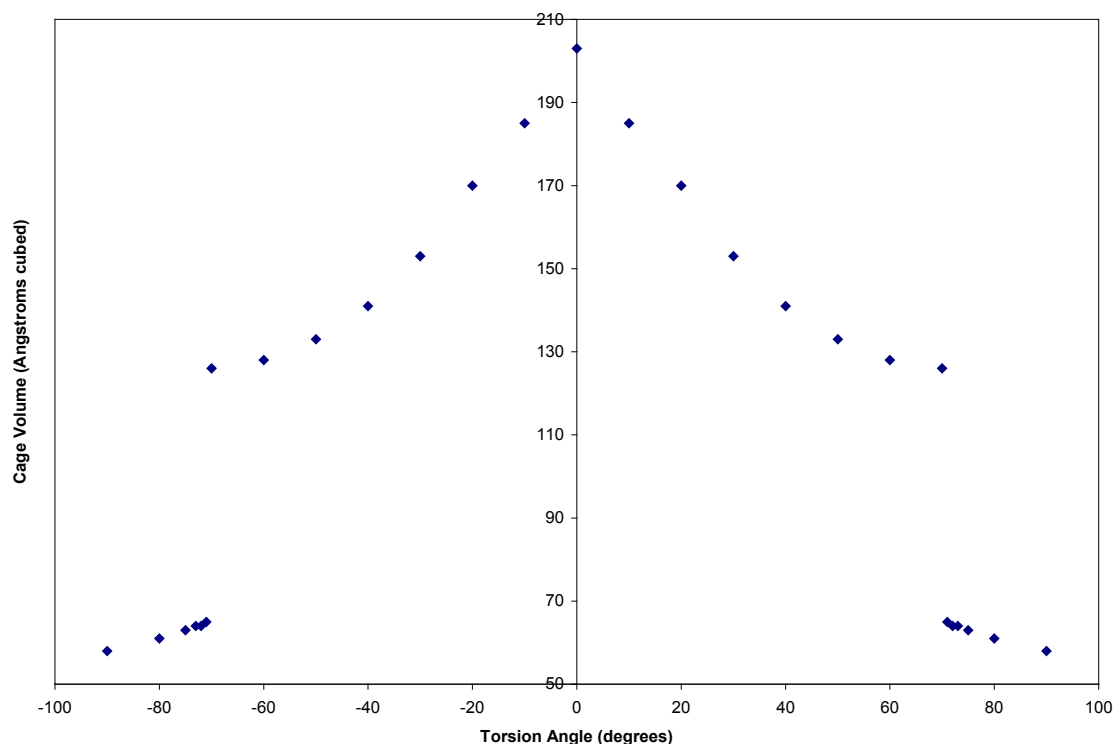


Figure S12: Plot of molecular modelling and volume calculation results.

1.7 Volume calculations.

These were performed with VOIDOO^{S20} using settings previously described.^{14,18-19} When the probe was found to “fall out” of the cavity the probe size was increased to the minimum size that would not escape.

1.8 Kinetics

1.8.1 PF_6^- diastereomer exchange

Single crystals of $[PF_6 \subset 1-T] \cdot 7PF_6 \cdot 9MeCN \cdot 3Et_2O$ were dissolved in CD_3CN and ^{19}F NMR spectra (376.45 MHz) were acquired at approximately 5 minute intervals for about 15 hours (Figure S12). The initial amount of diastereomers present was 94.6% T , 1.9% S_4 , and 3.5% C_3 based on peak integrals averaged over each component of the doublet. The T isomers decreased exponentially to an equilibrium value of 62.3%, while S_4 and C_3 increased exponentially to 22.3% and 15.4%, respectively, as is shown in Figure S14. The equilibrium values are in good agreement with the values from the 1H spectra.

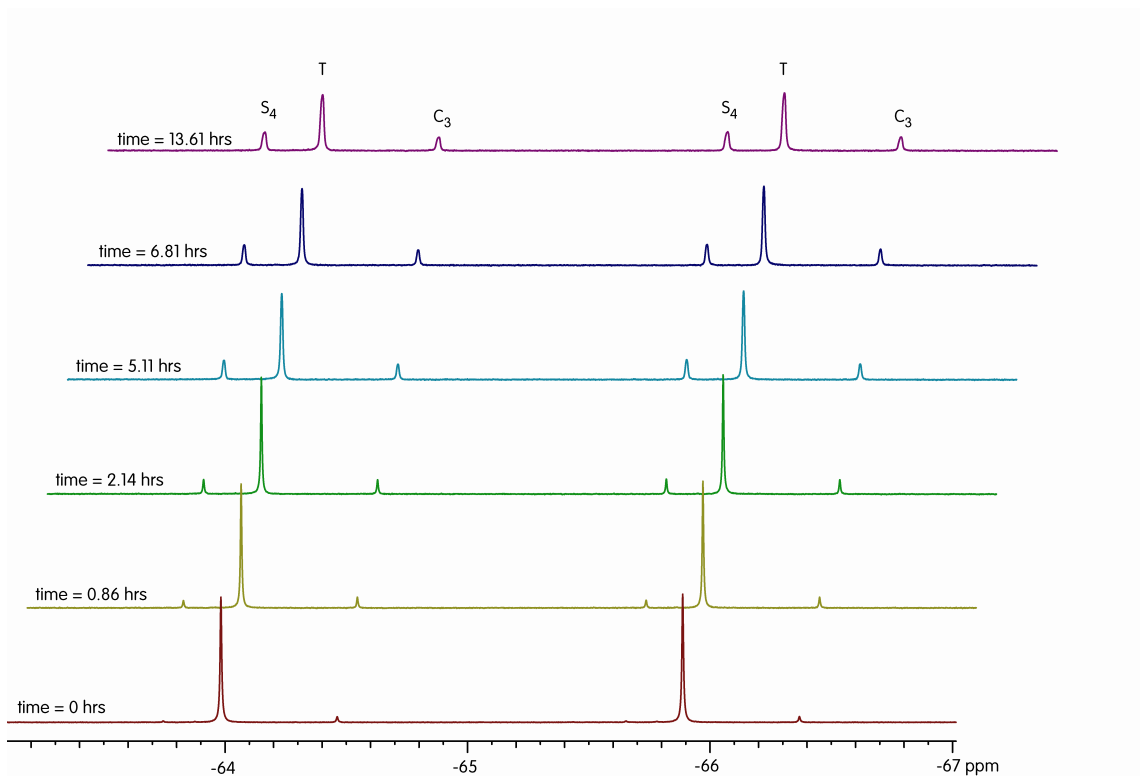


Figure S13: Selected ^{19}F NMR spectra showing the change in diastereomers over time from pure $1-T$.

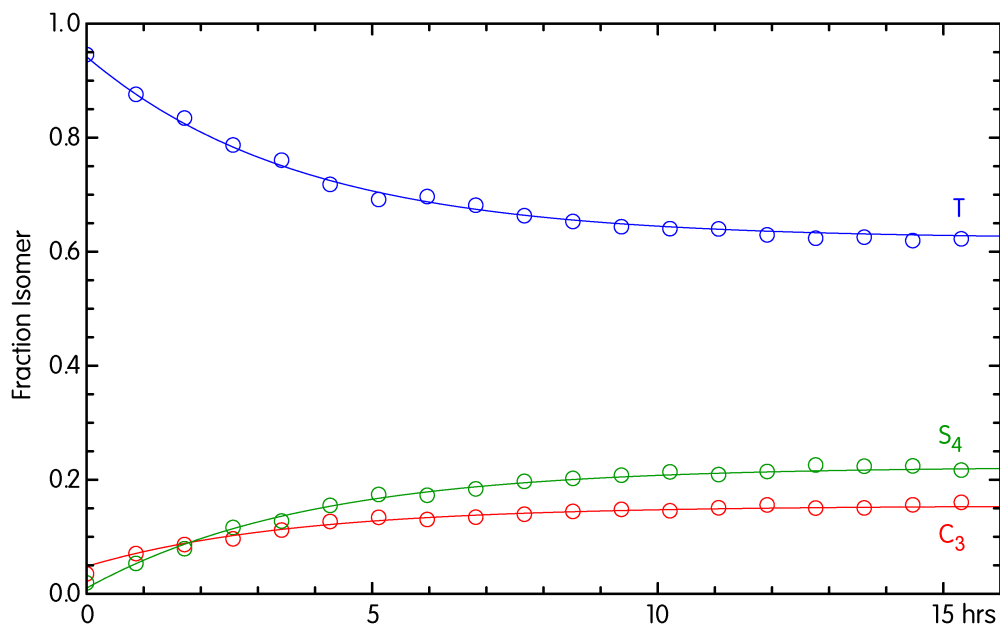
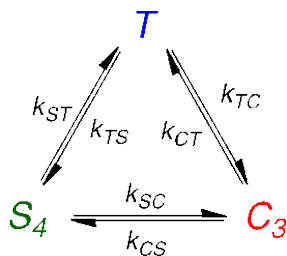


Figure S14: Fraction of *T*, *C*₃, and *S*₄ stereoisomers as a function of time.

The kinetics of diastereomer interconversion was modeled with a three site exchange that allowed forward and reverse reactions as show in Scheme S2.



Scheme S2. Rate constants for interconversion of diastereomer

The exchange of these three sites is given by

$$\frac{dT}{dt} = -(k_{TC} + k_{TS})T + k_{CT}C + k_{ST}S \quad (28a)$$

$$\frac{dC}{dt} = k_{TC}T - (k_{CT} + k_{CS})C + k_{SC}S \quad (28b)$$

$$\frac{dS}{dt} = k_{TS}T + k_{CS}C - (k_{ST} + k_{SC})S \quad (28c)$$

where *T*, *C* and *S* are the concentrations of the *T*, *C*₃, and *S*₄ diastereomers and the six *k*s are the microscopic rate constants. This can be expressed concisely in matrix form as

$$\frac{d\mathbf{C}}{dt} = \mathbf{K}\mathbf{C} \quad (29)$$

where \mathbf{C} is the column vector $\{T, C, S\}$ of the individual magnetizations and \mathbf{K} is the rate matrix

$$\mathbf{K} = \begin{pmatrix} -(k_{TC} + k_{TS}) & k_{CT} & k_{ST} \\ k_{TC} & -(k_{CT} + k_{CS}) & k_{SC} \\ k_{TS} & k_{CS} & -(k_{ST} + k_{SC}) \end{pmatrix} \quad (30)$$

Equation 29 has the following general solution

$$\mathbf{C}(t) = \mathbf{V}e^{+\lambda t} \quad (31)$$

where \mathbf{V} is the column of eigenvectors and λ is the diagonal matrix of eigenvalues. λ is essentially the diagonal form of the rate matrix \mathbf{K} and represents a transformation of coordinates according to $\lambda\mathbf{C} = \mathbf{K}\mathbf{C}$, which can be written as $(\mathbf{K}-\lambda\mathbf{I})\mathbf{C} = 0$. This equation has non-trivial solutions when its determinant is zero. Expansion of the determinant using the method of cofactors gives rise to the characteristic equation, in this case a third order polynomial, which has three roots, or eigenvalues. Substituting those eigenvalues into $(\mathbf{K}-\lambda\mathbf{I})\mathbf{C} = 0$ gives rise to three eigenvectors. The eigenvectors calculated by this method are not unique and can be scaled by any amount. Boundary conditions however determine the appropriate scaling factor for each eigenvector, such that is at time zero we know the individual concentration of T , C_3 , and S_4 . This gives rise to three equations with three unknowns, the scaling factors S_1 , S_2 , and S_3 , which can be solved for to give the concentrations at any arbitrary time t . Finally, the data are fit by varying the k s so as to minimize the deviations between the experimental and fitted concentrations. In this simulation only three rate constants were fitted; the remaining were determined from the known ratios of T , C_3 , and S_4 at equilibrium, i.e.

$$\mathbf{K} = \begin{pmatrix} -(k_{TC} + k_{TS}) & 3.970k_{TC} & 2.700k_{TS} \\ k_{TC} & -3.970k_{TC} - k_{CS} & 0.710k_{CS} \\ k_{TS} & k_{CS} & -2.700k_{TS} - 0.710k_{CS} \end{pmatrix} \quad (32)$$

The following Mathematica^{S21} program was written to find the desired rate constants.

```
Clear[S1, S2, S3, kTC, kTS, kCS]
dat = Import["all.csv", "Data"];
trange = 60000; A0 = 1;
(* subroutine to calculate concentration of T at any time t. *)
CT[kTC_, kTS_, kCS_, t_] :=
Module[{k, vals, vecs, sol, S1, S2, S3},
k = {{-kTC - kTS, 3.970 kTC, 2.700 kTS},
{kTC, -3.970 kTC - kCS, 0.710 kCS},
{kTS, kCS, -2.700 kTS - 0.710 kCS}};
vals = Eigenvalues[k];
vecs = Eigenvectors[k];
```

```

sol = Solve[{0.942 == S1*Part[vecs,1,1]+S2*Part[vecs,2,1]+S3*Part[vecs,3,1],
            0.048 == S1*Part[vecs,1,2]+S2*Part[vecs,2,2]+S3*Part[vecs,3,2],
            0.010 == S1*Part[vecs,1,3]+S2*Part[vecs,2,3]+S3*Part[vecs,3,3]},
            {S1,S2,S3}];
S1 = S1/.sol; S2 = S2/.sol; S3 = S3/.sol;
S1*Part[vecs,1,1]*Exp[Part[vals,1]*t] +
S2*Part[vecs,2,1]*Exp[Part[vals,2]*t] +
S3*Part[vecs,3,1]*Exp[Part[vals,3]*t]]
(* subroutine to calculate concentration of C3 at any time t. *)
CC3[kTC_, kTS_, kCS_, t_] :=
Module[{k, vals, vecs, sol, S1, S2, S3},
k = {{-kTC - kTS, 3.970 kTC, 2.700 kTS},
     {kTC, -3.970 kTC - kCS, 0.710 kCS},
     {kTS, kCS, -2.700 kTS - 0.710 kCS}};
vals = Eigenvalues[k];
vecs = Eigenvectors[k];
sol = Solve[{0.942 == S1*Part[vecs,1,1]+S2*Part[vecs,2,1]+S3*Part[vecs,3,1],
            0.048 == S1*Part[vecs,1,2]+S2*Part[vecs,2,2]+S3*Part[vecs,3,2],
            0.010 == S1*Part[vecs,1,3]+S2*Part[vecs,2,3]+S3*Part[vecs,3,3]},
            {S1,S2,S3}];
S1 = S1/.sol; S2 = S2/.sol; S3 = S3/.sol;
S1*Part[vecs,1,2]*Exp[Part[vals,1]*t] +
S2*Part[vecs,2,2]*Exp[Part[vals,2]*t] +
S3*Part[vecs,3,2]*Exp[Part[vals,3]*t]]
(* subroutine to calculate concentration of S4 at any time t. *)
CS4[kTC_, kTS_, kCS_, t_] :=
Module[{k, vals, vecs, sol, S1, S2, S3},
k = {{-kTC - kTS, 3.970 kTC, 2.700 kTS},
     {kTC, -3.970 kTC - kCS, 0.710 kCS},
     {kTS, kCS, -2.700 kTS - 0.710 kCS}};
vals = Eigenvalues[k];
vecs = Eigenvectors[k];
sol = Solve[{0.942 == S1*Part[vecs,1,1]+S2*Part[vecs,2,1]+S3*Part[vecs,3,1],
            0.048 == S1*Part[vecs,1,2]+S2*Part[vecs,2,2]+S3*Part[vecs,3,2],
            0.010 == S1*Part[vecs,1,3]+S2*Part[vecs,2,3]+S3*Part[vecs,3,3]},
            {S1,S2,S3}];
S1 = S1/.sol; S2 = S2/.sol; S3 = S3/.sol;
S1*Part[vecs,1,3]*Exp[Part[vals,1]*t] +
S2*Part[vecs,2,3]*Exp[Part[vals,2]*t] +
S3*Part[vecs,3,3]*Exp[Part[vals,3]*t]]
(*define chi squared error function *)
erfunc[kTC_, kTS_, kCS_, datum_] :=
(datum[[2]] - CS4[kTC, kTS, kCS, datum[[1]])^2 +
(datum[[3]] - CT[kTC, kTS, kCS, datum[[1]])^2 +
(datum[[4]] - CC3[kTC, kTS, kCS, datum[[1]])^2
chisq = Map[erfunc[kTC, kTS, kCS, #] &, dat];
(* Find ks that give minimum deviations with intial guesses *)
soln = FindMinimum[Abs[Apply[Plus, chisq]], {kTC, 0.0000123000},
                  {kTS, 0.0000149000}, {kCS, 0.0000100000}, Method -> "PrincipalAxis"]

```

The following rate constants were determined by this method

$$\begin{array}{ll}
 k_{TC} = 1.1 \pm 0.1 \times 10^{-5} \text{ s}^{-1} & k_{CT} = 4.2 \pm 0.2 \times 10^{-5} \text{ s}^{-1} \\
 k_{TS} = 1.6 \pm 0.1 \times 10^{-5} \text{ s}^{-1} & k_{ST} = 4.4 \pm 0.3 \times 10^{-5} \text{ s}^{-1} \\
 k_{CS} = 1.4 \pm 1.0 \times 10^{-6} \text{ s}^{-1} & k_{SC} = 1.0 \pm 1.0 \times 10^{-6} \text{ s}^{-1}
 \end{array}$$

1.8.2 NTf_2^- diastereomer exchange

Single crystals of $[1-S_4] \cdot 8NTf_2 \cdot 5MeCN \cdot 2H_2O \cdot Et_2O$ were dissolved in CD_3CN and 1H NMR spectra (500.13 MHz) were acquired at approximately 5 minute intervals for about 45 hours (Figure S14) although the reaction is largely over after 24 hours. Based on peak integrals of the imine hydrogens, the initial ratio of diastereomers was 0.0% T , 96.7% S_4 , and 3.3% C_3 . The S_4 isomer decreased exponentially to an equilibrium value of 49%, while T and C_3 increased exponentially to 41% and 10%, respectively (Figure S16).

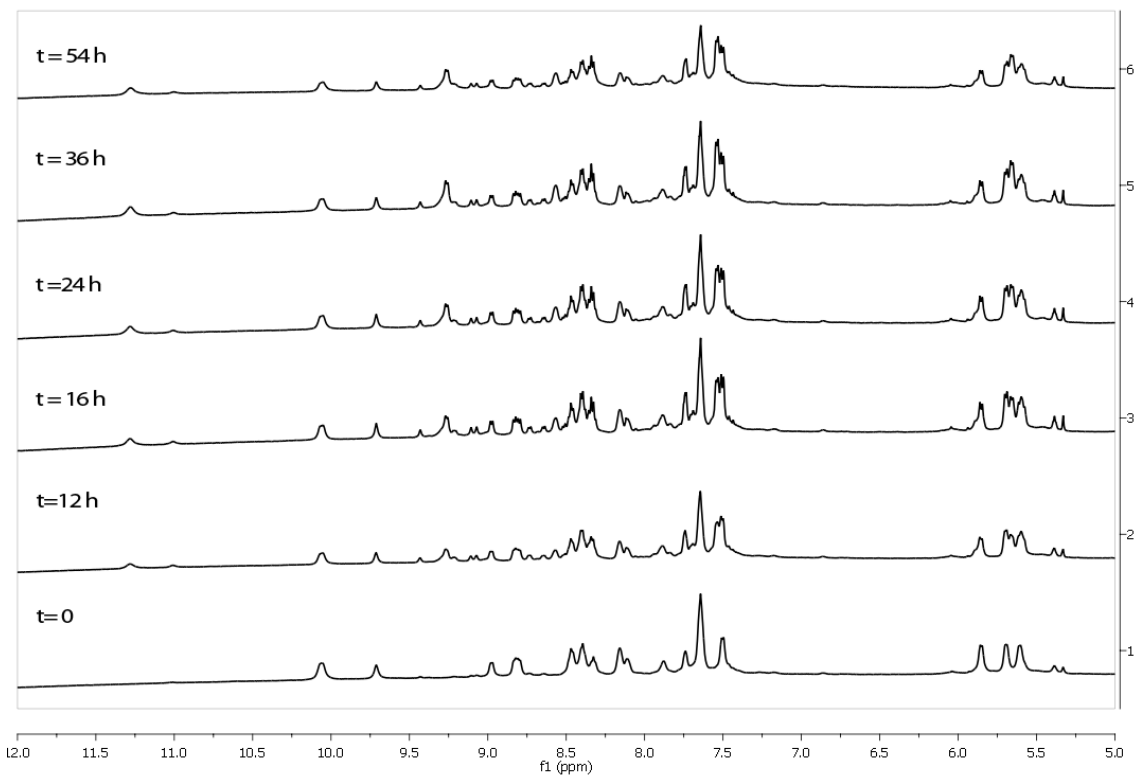


Figure S15: Representative 1H NMR (500 MHz, CD_3CN) spectra of the for single crystals of $[1] \cdot 8NTf_2$ showing diastereomer interconversion from $1-S_4$ at $t = 0$ to the equilibrium position after 42 hours.

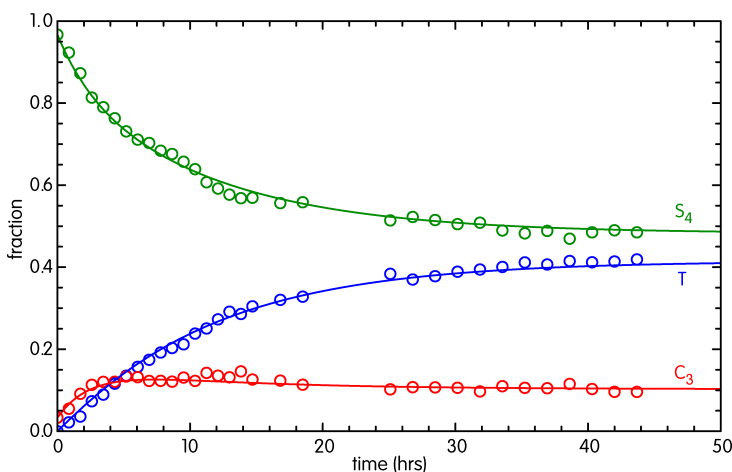


Figure S16. Fraction of T , C_3 , and S_4 stereoisomers as a function of time.

For the kinetic analysis every tenth data point (approximately 52 minute intervals) was processed in a manner similar to that described for the $[1] \cdot 8PF_6$ above. Using a similar *Mathematica* program but with boundary conditions appropriate for NTf_2 system, i.e. different populations at time = 0 and ∞ . The fit of the rate data resulted in the following rate constants:

$$\begin{aligned} k_{SC} &= 17 (\pm 2) \times 10^{-6} \text{ s}^{-1} & k_{CS} &= 77 (\pm 7.) \times 10^{-6} \text{ s}^{-1} \\ k_{ST} &= 8.6 (\pm 0.5) \times 10^{-6} \text{ s}^{-1} & k_{TS} &= 10.0 (\pm 0.6) \times 10^{-6} \text{ s}^{-1} \\ k_{CT} &= 19 (\pm 3.) \times 10^{-6} \text{ s}^{-1} & k_{TC} &= 4.7 (\pm 0.8) \times 10^{-6} \text{ s}^{-1} \end{aligned}$$

1.8.3 BF_4^- guest exchange monitored by 2D ^{19}F EXSY.

2D EXSY experiments were performed on a sample of $1 \cdot 8NTf_2$ in CD_3CN to which had been added 12 equivalents of $Bu_4N^+ BF_4^-$ to determine the rate constants for the exchange of BF_4^- into and out of cage **1**.

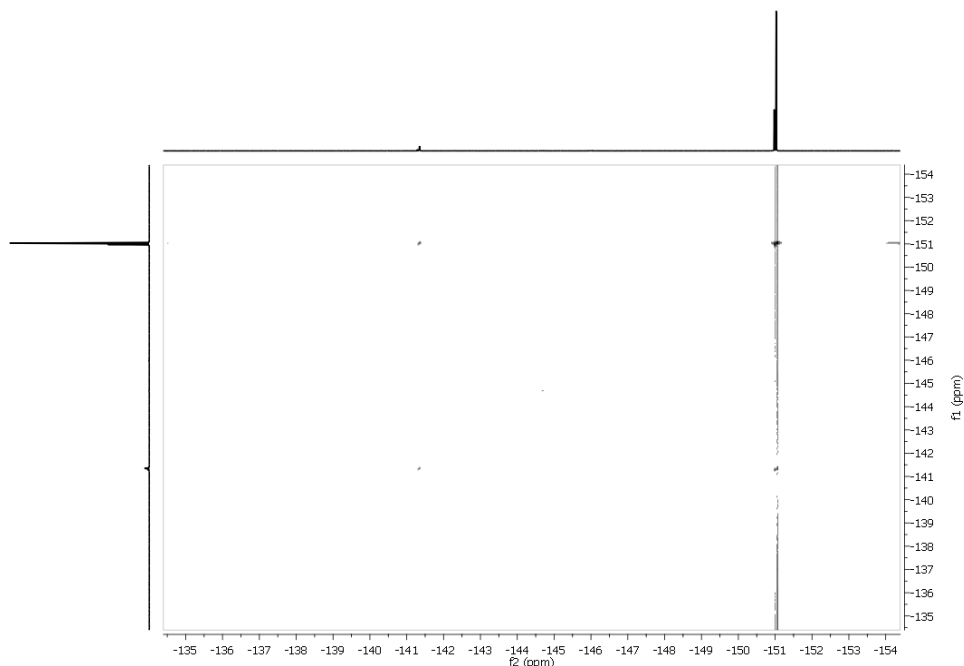


Figure S17: A 2D ^{19}F EXSY NMR for $[\text{BF}_4^-] \cdot 7\text{BF}_4$

The time dependent deviations of magnetization from equilibrium in a 2D EXSY experiment is given by:

$$\frac{dM_1}{dt} = -(R_{1,1} + k_{12})M_1 + k_{21}M_2 \quad (33a)$$

$$\frac{dM_2}{dt} = +k_{12}M_1 - (R_{1,2} + k_{21})M_2 \quad (33b)$$

which can be expressed concisely in matrix form as

$$\frac{d\mathbf{M}}{dt} = -\mathbf{R}\mathbf{M} \quad (34)$$

where \mathbf{M} is the column vector $\{M_1, M_2\}$ of the individual magnetizations and \mathbf{R} is the relaxation matrix that contains rate constants and spin-lattice relaxation times, T_I

$$\mathbf{R} = \begin{pmatrix} (T_{1,1}^{-1} + k_{12}) & -k_{12} \\ -k_{21} & (T_{1,2}^{-1} + k_{21}) \end{pmatrix} \quad (35)$$

Equation 34 has the following general solution at time equals t_{mix}

$$\mathbf{M}(t_{mix}) = \mathbf{M}_0 e^{-\mathbf{R}t_{mix}} \quad (36)$$

Equation 36 gives the intensity of peaks \mathbf{M} as a function of rate constants. We invert equation 36 to find the rates as a function of intensity following the method of Perrin and Gipe.²¹⁻²² First we solve for \mathbf{R}

$$\mathbf{R} = \frac{-\ln[\mathbf{M}(t_{mix})/\mathbf{M}_0]}{t_{mix}} = -\frac{\ln \mathbf{A}}{t_{mix}} \quad (37)$$

where \mathbf{A} is the matrix of NMR intensities from the 2D EXSY experiment

$$\mathbf{A} = \begin{pmatrix} \frac{I_{11}(t_{mix})}{I_{11}^0} & \frac{I_{12}(t_{mix})}{I_{22}^0} \\ \frac{I_{21}(t_{mix})}{I_{11}^0} & \frac{I_{22}(t_{mix})}{I_{22}^0} \end{pmatrix} \quad (38)$$

and $I_{ii}(t_{mix})$ are the diagonal peak intensities (as measured by their volumes), $I_{ij}(t_{mix})$ are the off-diagonal (cross) peak intensities, and I_{ii}^0 are the intensities at zero mixing time. These latter are proportional to the populations of the individual sites determined from the 1D spectrum. Next $\mathbf{M}(t_{mix})/\mathbf{M}_0$ is diagonalized using square matrix \mathbf{X} to give $\mathbf{\Lambda}$, so that the diagonal matrix $\ln \mathbf{\Lambda}$ has elements that are the logarithms of the eigenvalues of $\mathbf{M}(t_{mix})/\mathbf{M}_0$.

$$\mathbf{R} = -\frac{\ln \mathbf{A}}{t_{mix}} = -\frac{\mathbf{X}(\ln \mathbf{\Lambda})\mathbf{X}^{-1}}{t_{mix}} \quad (39)$$

A *Mathematica*^{S21} program was written to find the desired rate constants according to equation 39. The following example shows the analysis for the ¹¹B isotopologue with a mixing time of 0.8 sec.

```
A = {{0,0}, {0,0}};
Int = {{0, }, {0,0}};
P1 = 866000000.; (* free BF4 @ tmix=0 *)
P2 = 113130000.; (* bound BF4 @ tmix=0 *)
tmix = 0.8;
Int[[1, 1]] = 719910000.; (* free BF4 peak @ tmix *)
Int[[2, 1]] = 4957100.; (* cross peak @ tmix *)
Int[[1, 2]] = 4957100.; (* cross peak @ tmix *)
Int[[2, 2]] = 11491000.; (* bound BF4 @ tmix *)
MatrixForm[Int]
A[[1, 1]] = Int[[1, 1]]/P1;
A[[2, 1]] = Int[[2, 1]]/P1;
A[[1, 2]] = Int[[1, 2]]/P2;
A[[2, 2]] = Int[[2, 2]]/P2;
MatrixForm[A]
Evals = Eigenvalues[A]
Lambda = DiagonalMatrix[Log[Evals]]; MatrixForm[Lambda]

(* The eigenvectors are a pair of 1x2 column vectors, which
when put together form a square matrix. Mathematica treats
the two eigenvectors as simple lists (two 2x1 row vectors),
```

This puts the off diagonal elements in the wrong place.
To generate the correct eigenvectors use the Transpose function,
which swaps the off diagonal elements, i.e. $A_{ij} \rightarrow A_{ji}$, *)

```
Evecs = Transpose[Eigenvectors[A]]; MatrixForm[Evecs]
R = -Evecs.Lambda.Inverse[Evecs]/tmix; MatrixForm[R]
k12 = -R[[2,1]] (* extract rates from relaxation matrix *)
k21 = -R[[1,2]] (* extract rates from relaxation matrix *)
T1free = 1/(R[[1,1]] - k12) (* extract T1 from relaxation matrix *)
T1bound = 1/(R[[2,2]] - k21) (* extract T1 from relaxation matrix *)
```

Two-dimensional ^{19}F EXSY spectra were acquired using a phase sensitive NOESY pulse sequence with mixing times (τ_m) of 0.05, 0.10, 0.20, 0.40, 0.80, 1.6, and 3.2 sec. The integrated volumes for the diagonal and off-diagonal peaks, as well as those from the peaks taken at “zero” mixing time (10 ms), were used as intensities in the **A** matrix.

The presence of ^{10}B and ^{11}B isotopes gives rise to an intrinsic isotope shift rendering the BF_4^- isotopologues distinguishable in the ^{19}F NMR. This, plus the use of multiple mixing times, gave redundant measures of the rate constants. The apparent first order rate constant for encapsulation (k_{obs}) was found to be $0.020 \pm 0.002 \text{ s}^{-1}$, or at these concentrations a second order rate constant (k_{in}) of $5.65 \pm 0.6 \text{ M}^{-1} \text{ s}^{-1}$. The rate constant for escape from the cage was found to be (k_{out}) $0.148 \pm 0.015 \text{ s}^{-1}$. The ratio of k_f/k_r ($=k_{out}/k_{in} = 7.4$) is consistent with the complex's stoichiometry. No $^{10}\text{B}/^{11}\text{B}$ kinetic isotope effect was observed in this reaction.

1.8.4 Kinetics of PF_6^- addition to $[\text{I}-\text{S}_4]\cdot 8\text{NTf}_2$

$[\text{I}]\cdot 8\text{NTf}_2$ (9.4 mg, 1.9 μmol) was dissolved in CD_3CN (0.5 mL) and NMe_4PF_6 (37 μL of a 0.051 M stock solution, 1.9 μmol) was added. Encapsulation of PF_6^- could be monitored by either following the decrease in free PF_6^- or the increase in encapsulated PF_6^- in each of the three diastereomers by using ^{19}F as a reporter nucleus (Figure S14).

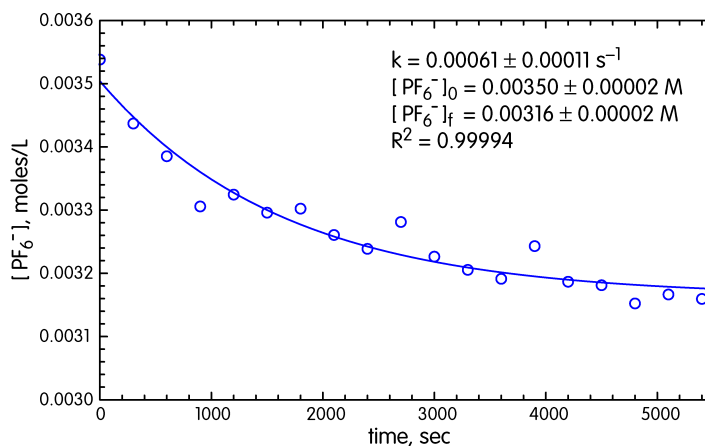


Figure S18: Decrease of free $[\text{PF}_6^-]$ as monitored by its ^{19}F doublet centered at -72.24 ppm.

The apparent first order rate constant for PF_6^- was determined by a non-linear least squares fit to the equations $[\text{PF}_6^-](t) = ([\text{PF}_6^-]_0 - [\text{PF}_6^-]_f) e^{-kt} + [\text{PF}_6^-]_f$ to be $k_{obs} =$

$0.00061 \pm 0.00011 \text{ s}^{-1}$, which gives a second order rate constant of $k_{in} = 0.172 \pm 0.031 \text{ M}^{-1} \text{ s}^{-1}$.

1.9 References

- S1. M. P. Sibi and G. Petrovic, *Tetrahedron: Asymmetry*, 2003, **14**, 2879-2882.
- S2. H. Schwenecke and D. Mayer, in *Ullmann's Encyclopedia of Industrial Chemistry*, Wiley-VCH, Weinhiem, 2005.
- S3. L. McGhee, R. M. Siddique and J. M. Winfield, *J. Chem. Soc., Dalton Trans.*, 1988, 1309-1314.
- S4. R. W. W. Hooft, COLLECT, Nonius B. V., Delft, The Netherlands, 1998
- S5. A. Technologies, CrysAlisPro, Agilent Technologies Ltd, Yarton, Oxfordshire, UK, 2009-2011
- S6. Rigaku, CrystalClear, Rigaku Americas and Rigaku Corporation., 9009 TX, USA 1997-2009
- S7. Z. Otwinowski and W. Minor, *Methods Enzymol.*, 1997, **276**, 307-326.
- S8. L. J. Farrugia, *J. Appl. Cryst.*, 1999, **32**, 837-838.
- S9. G. M. Sheldrick, SADABS: Empirical Absorption and Correction Software, University of Göttingen, Germany, 1996-2008
- S10. R. H. Blessing, *Acta Cryst.*, 1995, **A51**, 33-38.
- S11. A. Altomare, M. C. Burla, M. Camalli, G. L. Cascarano, C. Giocavazzo, A. Gaugliardi, G. C. Moliterni, G. Polidori and S. Spagna, *J. Appl. Cryst.*, 1999, **32**, 115-119.
- S12. L. Palatinus and G. Chapuis, *J. Appl. Cryst.*, 2007, **40**, 786-790.
- S13. G. M. Sheldrick, SHELX-97: Programs for Crystal Structure Analysis, University of Göttingen, Göttingen, 1997
- S14. P. van der Sluis and A. L. Spek, *Acta Crystallographica Section A*, 1990, **46**, 194-201.
- S15. A. L. Spek, PLATON: A Multipurpose Crystallographic Tool, Utrecht University, Utrecht, The Netherlands, 2008
- S16. S. J. Coles and P. A. Gale, *Chem. Sci.*, 2012, **3**, 683-689.
- S17. Y. R. Hristova, M. M. J. Smulders, J. K. Clegg, B. Breiner and J. R. Nitschke, *Chem. Sci.*, 2011, **2**, 638-641.
- S18. R. A. Bilbeisi, J. K. Clegg, N. Elgrishi, X. d. Hatten, M. Devillard, B. Breiner, P. Mal and J. R. Nitschke, *J. Am. Chem. Soc.*, 2012, **134**, 5110-5119.
- S19. Wavefunction, SPARTAN '10 for Windows, Wavefunction Inc, Irvine, CA USA, 2010
- S20. G. J. Kleywegt and T. A. Jones, *Acta Cryst.*, 1994, **D50**, 178-185.
- S21. Mathematica, Wolfram Research, Inc., Champaign, IL, USA, 2010